CRYSTAL GROWTH & DESIGN
2006
VOL. 6, NO. 7
1575−1583

Sodium Sulfate Crystallization in the Presence of Phosphonates: Implications in Ornamental Stone Conservation

Encarnación Ruiz-Agudo,† Carlos Rodriguez-Navarro,* and Eduardo Sebastián-Pardo†

Department Mineralogía y Petrología, Universidad de Granada, Fuentenueva s/n, 18002 Granada, Spain

Received September 28, 2005; Revised Manuscript Received May 17, 2006

ABSTRACT: Phosphonates were tested as potential crystallization inhibitors for sodium sulfate, one of the most damaging soluble salts in historic building and sculpture. Although mirabilite ($Na_2SO_4 \cdot 10H_2O$) crystallization is promoted in the presence of 1-hydroxyethylidene-1,1-diphosphonic acid (HEDP), aminotris(methylenephosphonic acid) (ATMP), and diethylenetriaminepentakis-(methylphosphonic acid) (DTPMP) at salt solution natural pH (6.4), crystallization is inhibited at moderately alkaline pH (8−8.5). Molecular modeling of additive adsorption on specific mirabilite (*hkl*) faces, in addition to ESEM observations, allowed us to identify how phosphonates inhibit mirabilite crystallization. ATMP and DTPMP display the best stereochemical matching with mirabilite {100} surfaces, which explains why they are the most effective inhibitors. Inhibition of sodium sulfate crystallization in the presence of phosphonates may promote the growth of efflorescence on porous ornamental stone, rather than damaging subefflorescence. The use of phosphonates may lead to more efficient preventive conservation of ornamental stone exposed to sodium sulfate damage.

Introduction

The crystallization of soluble salts is known to contribute to rock decay in many natural environments (e.g., coastal areas, arid and desert regions, and Antarctica).[1,2] Salt weathering is also a substantial hazard for historic architecture and statuary, in addition to modern buildings and engineering structures.[3,4,5] Typical soluble salts associated with this type of weathering include chlorides, sulfates, and nitrates of alkali and alkaline-earth metals.[1] Salt damage is due to the pressure exerted by a salt crystal when it grows inside a confined space: i.e., a pore.[5a−7] This pressure easily exceeds the rupture modulus of most ornamental porous materials and thus leads to their crumbling and disintegration.[2,8]

The application of methods which mitigate or prevent salt weathering in ornamental stone has been the subject of much research.[9] However, most of the conservation methods applied to date have only been partially successful. The most common strategies for the prevention or minimization of salt damage include the implementation of tight environmental control[10] and the use of traditional organic consolidants or protective coatings.[11] However, it is not yet feasible to place historic buildings within environments in which temperature and relative humidity can be controlled. Nor have traditional treatments such as consolidation yielded better solutions, since in most cases they do not arrest salt weathering but only cover up its effects.

Recently, it has been proposed that additives which modify the crystallization process could be used to halt and/or mitigate salt weathering.[12−14] These additives can inhibit or promote salt crystallization within a pore. In the first case, an increase is observed in the period between the establishment of supersaturation and the formation of a new phase at a higher critical supersaturation.[15] Such increased induction times make it possible for the saline solution to reach the surface of the porous stone prior to the onset of crystallization. Once the solution reaches the surface, crystallization of harmless efflorescence takes place.[14] In contrast, when additives promote crystallization, salt precipitation occurs within the pores at low supersaturation and, thus, crystallization pressure is reduced.[12] As a consequence, damage to the substrate is minimized.[14]

Examples of crystallization additives with technological and industrial uses are phosphates and polyphosphates,[16−18] carboxylic acid derivatives,[19−22] polyelectrolytes,[17,20,23,24] ferrocyanides,[13,14] and phosphonates.[25−30] The last species are among the most common crystallization inhibitors. Phosphonates have been applied as scale and corrosion control additives, as well as dispersants, cleaning agents, chelating agents, and crystal growth modifiers.[31] The application of phosphonates has made it possible to control the crystallization of sparingly soluble phases, such as calcium carbonates[27,29,32,33] and barium, strontium, and calcium sulfates,[15,19,21,22,30,34−39] which pose significant problems in the oil industry and in water treatment. Phosphonates have also been used to control pyrite,[40] ettringite,[41] calcium silicate hydrate,[42] and hydroxyapatite[43] precipitation.

However, very little is known about the effects of phosphonates on the crystallization of damaging soluble salts, particularly those of alkali metals. Some research has focused on the crystallization of LiBr in the presence of phosphonates.[44,45] However, LiBr has never been associated with salt weathering phenomena. With the exception of the preliminary results of Selwitz and Doehne,[13] no other studies appear to have dealt with the effects of phosphonates on the precipitation of highly soluble salts such as sodium sulfate.

Sodium sulfate has been found to be particularly damaging to modern cement structures, as well as to porous stone in historical buildings.[6,12] This is apparently due to the generation of high crystallization pressure,[1,2] which is associated with the ability of this salt to form highly supersaturated solutions with respect to the decahydrated phase (mirabilite).[46] Its deleterious effects have made sodium sulfate the chosen salt in accelerated decay tests performed to evaluate the durability of building materials.[47] On the other hand, sodium sulfate is used as a filler for household detergents, and in paper-pulp and glass manufacturing.[48] Aqueous solutions of sodium sulfate have been employed in heat storage devices, due to their high latent heat storage density and low cost.[49] However, sodium sulfate crystallization is still not fully understood,[12a] despite the amount of research devoted to this salt. Apparently, this is due to the complexity of the $Na_2SO_4-H_2O$ system. The system includes

* To whom correspondence should be addressed. E-mail: carlosrn@ugr.es. Tel: + 34 958 246616. Fax: + 34 958 243368.
† E-mail: encaruiz@ugr.es (E.R.-A.); rolando@ugr.es (E.S.-P.).

10.1021/cg050503m CCC: $33.50
Published on Web 06/20/2006

two stable phases, thenardite (Na_2SO_4) and mirabilite ($Na_2SO_4 \cdot 10H_2O$), and a metastable phase, sodium sulfate heptahydrate ($Na_2SO_4 \cdot 7H_2O$), which has not yet been clearly identified in nature.[12a] Research regarding the interactions of crystallization inhibitors and sodium sulfate crystals is therefore challenging because of the complex characteristics of this system.

It is the aim of this work to study the effects of various organophosphonic acids on the crystallization of sodium sulfate. We have investigated the dynamics and kinetics of sodium sulfate crystallization in the presence of HEDP (1-hydroxyethylidene-1,1-diphosphonic acid), ATMP (aminotris(methylenephosphonic acid)) and DTPMP (diethylenetriaminepentakis-(methylphosphonic acid)), three of the most common phosphonates used as crystallization inhibitors. These additives were selected because they differ in the number of phosphonate groups (2, 3, and 5) and nitrogen atoms (0, 1, and 3). Particular attention has been given to the role of chemical and structural factors regarding the effects of the additives in sodium sulfate crystallization. Finally, we have also attempted to determine whether these additives could be used to control salt weathering.

Materials and Methods

(a) Batch Crystallization Tests. These tests were carried out using a special laboratory setup which enables crystallization of sodium sulfate solution in glass crystallizers (500 mL Pyrex). Crystallization took place following free evaporation in an environmentally controlled chamber ($T = 20 \pm 2$ °C; HR $= 40 \pm 10\%$). Details of the laboratory setup have been published elsewhere.[14] Additional tests were carried out using silicone grease covered glass crystallizers in order to determine the influence of the substrate on crystallization. The effect of pH on sodium sulfate crystallization in the presence of phosphonates was determined by tests using pH values ranging from 5 to 9.

For each batch crystallization test, 250 mL of saturated sodium sulfate solution was prepared using anhydrous solid (Panreac, analytical grade) and deionized water (with conductivity less than 50 μS/cm). The saturated solution was decanted to remove any undissolved crystals. HEDP, ATMP, and DTPMP were obtained from Fluka (reagent grade) and used as received. Additives were added to the saturated solution at working concentrations of 10^{-4}, 10^{-3}, and 10^{-2} M. The selected additives acidify the saturated sodium sulfate solution, and the pH was thus adjusted to the target pH using NaOH solution. The solution was then poured into the glass crystallizers and allowed to evaporate. A control (saline solution without additive) was placed in each crystallization run. Up to 109 tests were performed (including controls and replicates).

The evaporation rate and supersaturation were evaluated on the basis of online weight loss and conductivity measurements (Orion, Model 635). These measurements enabled the determination of induction time and critical relative supersaturation. The induction time is defined as the interval between the start of the experiment and the onset of crystallization. The critical relative supersaturation, σ, is defined as the supersaturation reached at the onset of crystallization and is calculated as $\sigma = 100(C - C_0)/C_0$, where C and C_0 are the actual and the saturation concentrations.[14] Runs in which the critical relative supersaturation of the control solution was under 30% were discarded in order to eliminate the seed effect (due to accidental decanting of solids).

(b) X-ray Diffraction Analysis (XRD). A Philips PW-1710 diffractometer with an automatic slit was used to identify which sodium sulfate phase(s) precipitated. Precipitates were collected immediately after crystallization and analyzed while still wet. Measurement parameters were as follows: Cu Kα radiation ($\lambda = 1.5405$ Å), an exploration range of 10 to 70° in 2θ, steps of 0.028° in 2θ, and a goniometer speed of 0.01° s^{-1} in 2θ.

(c) Environmental Scanning Electron Microscopy (ESEM). A Philips Quanta 400 ESEM instrument was used to determine the habit and size distribution of sodium sulfate crystals. Microtextural and morphological modifications of the salt after dissolution and recrystallization in the absence and presence of additives were studied in situ. Condensation and evaporation of water on salt samples were produced by modifying the temperature (Peltier stage) and gas pressure (water vapor) inside the ESEM chamber (P, 3.5−6.5 Torr; T, 2−8 °C; relative humidity, ~31.9−94.2%).[5b] Time-lapse digital images were recorded on line.

Unlike conventional SEM, ESEM enables the observation of the different phases of sodium sulfate at high magnification and without changing their hydration state, morphology, and/or habit.[5b] Textural and/or morphological differences of hydrated salt crystals formed in the presence of additives can also be observed, as well as real-time changes during crystallization or hydration/dehydration events. ESEM therefore enables the dynamic study of crystallization processes, and since it facilitates more precise analysis of salt weathering,[5b,12] it is gaining prevalence in cultural heritage conservation.

(d) Molecular Modeling. The MSI Cerius^2 computer program was used to model the crystal surface−additive interactions by a force-field approach. Cerius^2 is a program package that uses empirical force-field potentials to calculate the total energy of atoms.[39] The universal force field (UFF)[50−52] was selected, since it provides a versatile parametrization for a wide range of atoms. UFF is a purely diagonal and harmonic force field. Bond stretching is described by a harmonic term, angle bending by a three-term Fourier cosine expansion, and torsion and inversion by cosine-Fourier expansion terms. van der Waals interactions are described by the Lennard−Jones potential. The electrostatic interactions are described by atomic monopoles and a screened (distance-dependent) Coulombic term. Cerius^2 includes bond, angle, torsion, van der Waals, and Coulomb energy terms in the UFF expression. The charge equilibration method,[53] which is part of the Cerius^2 package, was used to calculate the charge distribution within the inhibitor molecules. Charge distribution determined by this method is highly dependent on molecule geometry. It is thus important to minimize the structure before calculation. Once the structure was minimized using UFF, the charge equilibration method was applied to the respective neutral molecule. Protons were subsequently removed, and the corresponding charge was adjusted by evenly distributing the charge difference over the remaining charged molecule. pK values were used to calculate the speciation of the additives. For each phosphonic acid, the main ionic species at the pH of maximum growth inhibition was selected to model inhibitor/crystal interactions.

Mirabilite crystal equilibrium morphology was calculated using the Bravais−Friedel−Donnay−Harker (BFDH) algorithm[54] (included in Cerius^2). The BFDH algorithm should be considered empirical, since it does not take into account the energetics of ion attachment. What this algorithm thus provides is an approximation to the crystal morphology based on a set of geometrical rules.[38]

The stereochemical matching of additives on mirabilite was modeled in several steps. First, surface cells were created from the mirabilite unit cell at a given Miller plane (cleavage plane). This surface cell was further extended to a block of four cells. Spacing was then measured between neighboring Na atoms, H atoms, and sulfate groups, on different crystal faces. Afterward, O−O and P−P distances were determined between different deprotonated functional groups of additives. Finally, stereochemical matching on specific mirabilite (*hkl*) planes was performed by replacing two sulfate groups with two phosphonate groups or by bonding two additive functional groups to (a) two Na atoms or (b) two H atoms. Degrees of mismatching of over 1% were not considered acceptable.

Results and Discussion

(a) Critical Supersaturation and Induction Iime at the Natural pH (6.4) of the Solution. Effect of Additive Concentration. To compare the additives, the critical supersaturation data were normalized with respect to the control critical supersaturation by using the *percentage of growth inhibition (GI).*[55] The latter is calculated here from the formula

$$\mathrm{GI} = \frac{\sigma_{\mathrm{additive}} - \sigma_{\mathrm{blank}}}{\sigma_{\mathrm{blank}}} \times 100 \qquad (1)$$

where $\sigma_{\mathrm{additive}}$ and σ_{blank} are the critical relative supersaturations in the presence and in the absence of the additive, respectively.

Conductivity measurements were valid to determine the onset of crystallization, but only in some cases. In most of the tests no significant changes were detected in solution conductivity

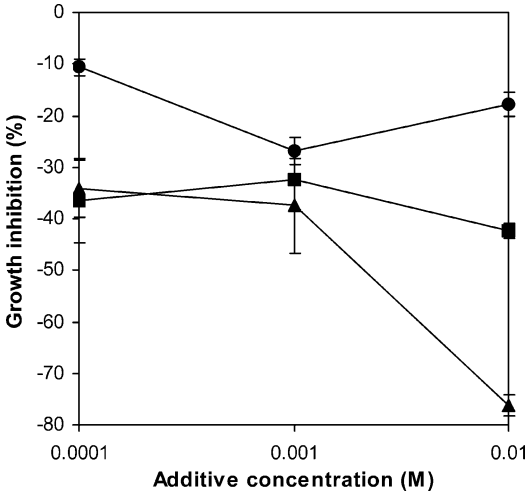

Figure 1. Percentage of growth inhibition vs inhibitor concentration (at pH ~6.5) for saturated sodium sulfate solutions: (●) ATMP; (■) HEDP; (▲) DTPMP. Values are averages of three replicates; error bars indicate standard deviations.

after the onset of crystallization. Crystallization onset was detected visually. Since GI values were used for comparison purposes, eventual (systematic) errors associated with visual detection of crystallization onset should not affect the interpretation of the results. In fact, visual detection of salt crystallization onset was highly reproducible; i.e., standard deviations of GI values were systematically bellow ±9%. Regarding the accuracy of visual detection compared with other techniques, Martin et al. found no significant differences in induction times determined by visual detection, transmittance, and conductivity measurements.[56]

Sodium sulfate decahydrate—mirabilite—was the only phase formed in the batch crystallization tests and was identified by XRD. Mirabilite crystallization was promoted by HEDP, ATMP, and DTMP when added to a saturated salt solution neutralized at ca. pH 6.4, which is the natural pH of saturated sodium sulfate solution. The critical supersaturation reached at working additive concentrations (10^{-2}, 10^{-3}, and 10^{-4} M) was systematically lower than that of the control solution (Figure 1). No clear trend was observed in crystallization promotion associated with additive concentration. Nonetheless, in the cases of ATMP and DTPMP, growth inhibition values became lower with increasing additive concentration.

Crystallization promotion may be due to a process involving sodium sulfate heterogeneous nucleation on the phosphonate-covered glass support. The silica glass−water interface is characterized by acid Si−OH groups because of the unsatisfied chemical O^- bonds at the silicate glass surface.[57] The point of zero charge (PZC) of silica is pH 1.8−3.[58,59] Hydroxyl groups thus deprotonate at pH >PZC and render the glass surface increasingly negative as pH rises. Therefore, phosphonate adsorption is promoted on the glass substrate via hydrogen bonds.[60] Such interaction would take place through phosphonic and Si−OH groups. This process may be enhanced via H bonds between Si−OH groups and the amino groups in ATMP and DTPMP.[60] It is well-known that phosphonates have a strong tendency to adsorb onto a variety of surfaces, including silicates (silica and clay minerals), calcite, barite, cassiterite, aluminum oxides, and iron oxides.[31,61] In some instances adsorption results in the formation of self-assembled monolayers of organophosphonic acids.[62,63] Such adsorbed layers may act as a template for mirabilite nucleation. Note that template-directed nucleation has been observed in a range of natural (e.g., biominerals) and artificial systems.[64] Template-directed nucleation of sodium sulfate is consistent with the systematic precipitation of mirabilite crystals on the surfaces of the glass crystallizers. This template effect may reduce the critical supersaturation at pH 6.4. However, no template effect appears to be plausible at higher pH, since both the phosphonate molecules and the silica glass surface become highly deprotonated and lead to electrostatic repulsion. In fact, phosphonate adsorption on different substrata is limited by increasing pH.[61]

Table 1. Percentage of Growth Inhibition (GI in %) of 0.001 M ATMP, HEDP, and DTPMP at Neutral pH (~6.4) in the Presence of Different Substrates[a]

substratum	HEDP	ATMP	DTPMP
glass	−32.4 ± 5.9	−26.7 ± 2.6	−37.4 ± 9.1
silicone	−88.1 ± 3.2	−33.9 ± 0.1	−25.9 ± 4.1

[a] The values given are averages of three replicates per run, and standard deviations are presented.

(b) Substrate Effect. Additional tests were carried out using silicone grease covered crystallizers, since it was assumed that the high amount of Si−OH bonds in the silicone[65] would enhance heterogeneous nucleation via adsorption of phosphonates. These tests showed increased promotion of mirabilite crystallization in the presence of the additives at pH 6.4 (Table 1). Silicone grease is a linear polymer and consists of chains of alternating dimethylsilylene units and oxygen atoms, $(-SiMe_2-O-)_x$, with terminal Si−OH groups.[65] Silicone grease is generally regarded as chemically inert toward most common reagents and solvents, although the polar silicon−oxygen bond is known to be reactive toward alkaline and acidic reagents. In recent years several cases of serendipitous participation of silicone grease in a number of reactions have been reported.[65] As in the case of silica glass, phosphonate behavior in the presence of silicone grease appears to be due to H bonding between the additive and silicone Si−OH groups. Adsorbed phosphonic acid derivatives will thus act as a "template" on which sodium sulfate crystals can grow. These molecules may promote template-directed heterogeneous nucleation of sodium sulfate.[66] Note that crystallization promotion on silicone grease was much greater in the presence of HEDP and was slightly increased in the case of ATMP but was similar to that of the clean glass test for DTPMP (Table 1). At pH 6.4 DTPMP displays the highest degree of deprotonation (six protons), while HEDP has the lowest (two protons) (see part c below). A high degree of deprotonation limits adsorption of phosphonate molecules on the silicon substrate via H bonding. This may help to account for the results presented in Table 1.

The effect of crystallization promotion suggests that there is some structural matching between sodium sulfate crystals and the additives. Such molecules could not otherwise act as a template for mirabilite crystallization. These phosphonates could minimize damage due to sodium sulfate crystallization when used in silicate-rich stones such as sandstones or those treated with ethyl silicate or silicones. Silicones and ethyl silicate are common consolidants and protective coatings used in stone conservation.[11] Damage minimization may occur because of the direct relation between crystallization pressure and critical supersaturation.[5a] The crystallization pressure, P, exerted by a salt when growing in a confined space, such as a pore, can be calculated by applying the Correns equation[5a]

$$P = \frac{RT}{V_m} \ln \frac{C}{C_0} \qquad (2)$$

where R is the ideal gas constant, T is the temperature, V_m is the molar volume of the salt, and C/C_0 is the supersaturation.

(c) pH Effect. A rise in pH led to increased inhibition capacity on sodium sulfate precipitation up to pH 8−8.5 (Figure 2). The affinity of an inhibitor to be adsorbed on the crystal depends on its capacity to be attracted to the surface and to be bound to it.[67] At higher pH, when phosphonate groups are highly deprotonated (Figure 3), the interaction reaches a maximum, since the inhibitor is electrostatically attracted and may establish bonds with the cations of a given crystal face.[26] Note, however, that upon further pH increase the degree of inhibition became lower (Figure 2).

The distribution of ionic species for ATMP, HEDP, and DTPMP was calculated at 25 °C using published pK values (Table 2).[68,69] The dissociation reactions are

$$\text{for ATMP: } H_nX^{(6-n)-} \overset{K_n}{\longleftrightarrow} H_{n-1}X^{(6-n+1)-} + H^+ \quad (3)$$

$$\text{for HEDP: } H_nY^{(4-n)-} \overset{K_n}{\longleftrightarrow} H_{n-1}Y^{(4-n+1)-} + H^+ \quad (4)$$

$$\text{for DTPMP: } H_nZ^{(10-n)-} \overset{K_n}{\longleftrightarrow} H_{n-1}Z^{(10-n+1)-} + H^+ \quad (5)$$

The various pK values refer to the equations

$$\text{for ATMP } (n = 1-6): \; K_n = \frac{[H^+][H_{n-1}X^{(6-n+1)-}]}{[H_nX^{(6-n)-}]} \quad (6)$$

$$\text{for HEDP } (n = 1-4): \; K_n = \frac{[H^+][H_{n-1}Y^{(4-n+1)-}]}{[H_nY^{(4-n)-}]} \quad (7)$$

$$\text{for DTPMP } (n = 1-10): \; K_n = \frac{[H^+][H_{n-1}Z^{(10-n+1)-}]}{[H_nZ^{(10-n)-}]} \quad (8)$$

The pK_n is given by the equation

$$pK_n = -\log K_n \quad (9)$$

The mass balances of the additives are

$$\text{for ATMP: } \sum_{n=1}^{n=7}[H_{n-1}X^{(6-n+1)-}] = C_{\text{TOTAL}} \quad (10)$$

$$\text{for HEDP: } \sum_{n=1}^{n=5}[H_{n-1}Y^{(4-n+1)-}] = C_{\text{TOTAL}} \quad (11)$$

$$\text{for DTPMP: } \sum_{n=1}^{n=11}[H_{n-1}Z^{(10-n+1)-}] = C_{\text{TOTAL}} \quad (12)$$

Figure 3 shows the distribution of ionic species for the three phosphonates. Despite the fact that saturated sodium sulfate solutions have a high ionic strength, no attempt was made to correct pK values. Note that Tomson et al. have shown that there are no significant changes in the distribution of phosphonate ionic species due to increased ionic strength (from 0.01 M up to 2 M).[69] Nevertheless, pK values would be only slightly reduced by an increase in ionic strength.

Phosphonate groups in inhibitor molecules are highly deprotonated at pH ∼8.5 (Figure 3), which is when the additives displayed their maximum inhibitory capacity. Higher pH values do not lead to significant changes in the distribution of ionic species. The pH would have to be extremely high in order to obtain a more deprotonated species. Total ionization, however, prevents the adsorption of the additive, because the energy gained by bonding to the crystal surface cannot compensate for the attendant entropy loss.[70] On the other hand, studies of various phosphonic acid derivatives over a wide pH range have shown that the presence of both deprotonated and protonated phosphonate groups leads to stronger interaction between adsorbed inhibitor molecules and crystal surfaces.[43] Both of the latter conclusions could help explain why GI percentages are lower at pH >8.5. However, the dominant ATMP and DTPMP ionic species at the highest pH tested (pH 9) are the same as those present at pH 8−8.5, when maximum inhibition is reached. Hence, it is unlikely that a change in the inhibition capacity at these moderately alkaline pH values is related to the protonation state of the additive. Therefore, other explanatory possibilities were explored. First, it should be considered that the salt crystal surface becomes increasingly negative and may thus electrostatically repel the ionized inhibitor molecules as the pH rises. It has been claimed that the latter effect accounts for the reduction in nucleation inhibition in the case of $BaSO_4$ precipitation at high pH.[30] Another possibility is that the crystal surface loses hydration water protons, therefore limiting its hydrogen-bonding capacity with the inhibitor molecule.[30] However, our molecular modeling (see part e below) suggests that growth inhibition occurs regardless of the establishment of hydrogen bonds between the additive and mirabilite crystal surface(s). We therefore propose that at pH >8.5 increased repulsive electrostatic forces between additive molecules and mirabilite crystals limit phosphonate inhibition.

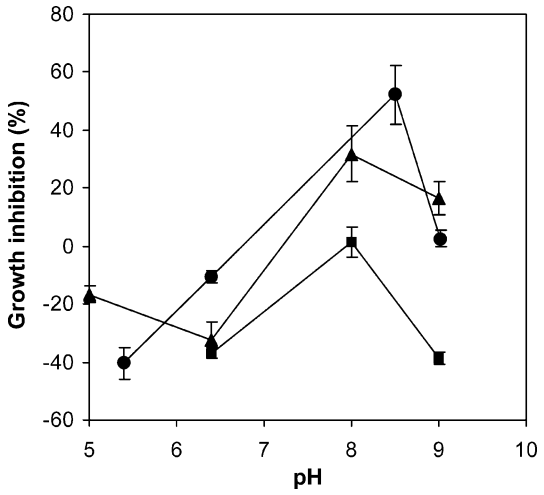

Figure 2. Percentage of growth inhibition vs pH of saturated sodium sulfate solutions: (●) 0.0001 M ATMP; (■) 0.001 M HEDP; (▲) 0.001 M DTPMP. Values are averages of three replicates; error bars indicate standard deviations.

Table 2. Protonation Constants of ATMP, HEDP, and DTPMP

	ATMP[a]	HEDP[a]	DTPMP[b]
log K_1	12.5 ± 0.2	11.0 ± 0.2	12.58
log K_2	7.22 ± 0.03	6.9 ± 0.1	11.18
log K_3	5.90 ± 0.02	2.7 ± 0.1	8.30
log K_4	4.59 ± 0.03	1.6 ± 0.2	7.23
log K_5	1.6 ± 0.3		6.23
log K_6	0.5 ± 0.3		5.19
log K_7			4.15
log K_8			3.11
log K_9			2.08
log K_{10}			1.04

[a] Data from ref 68. Conditions: I = 0.1 mol L^{-1} (KNO_3), 25 ± 0.5 °C. [b] Data from ref 69.

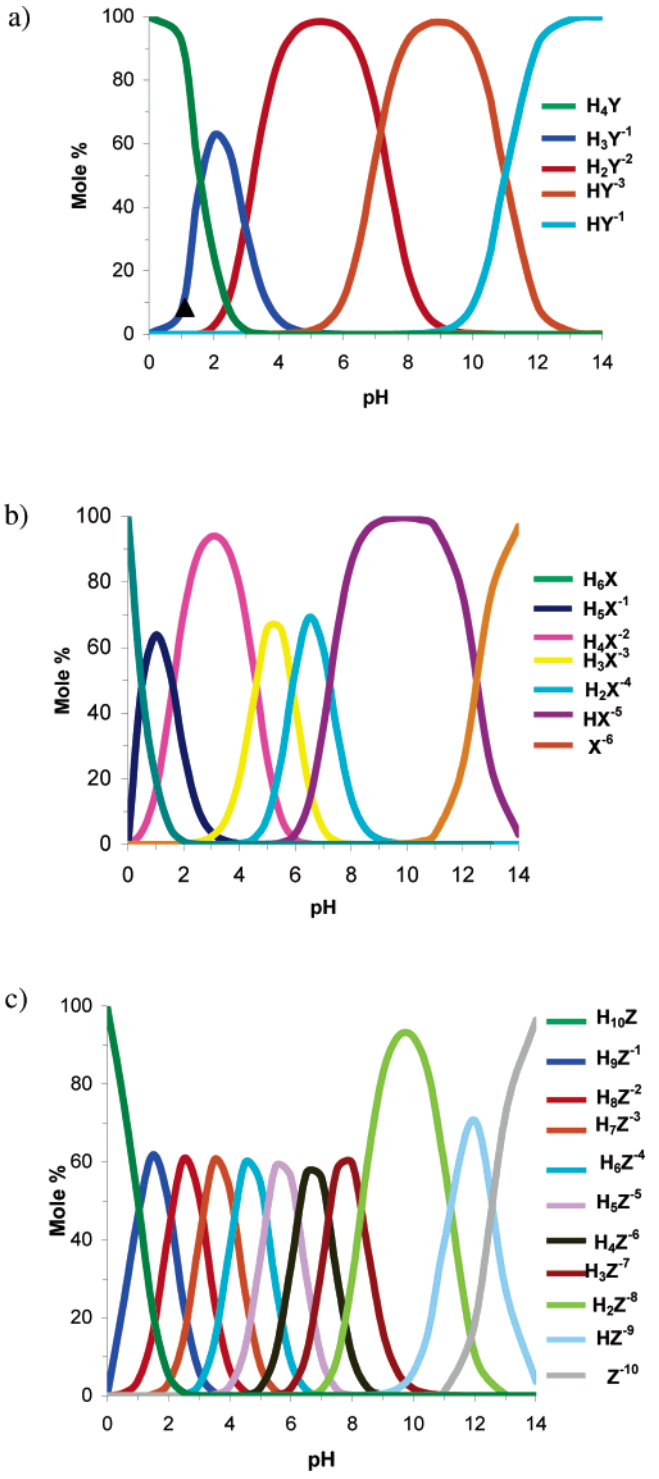

Figure 3. Distribution of phosphonate ionic species as a function of pH: (a) HEDP; (b) ATMP; (c) DTPMP.

Our results at pH 8−8.5 show that a higher number of phosphonate groups does not guarantee that a molecule will have greater inhibition capacity. This can be observed in the case of ATMP and DTPMP. While DTPMP has five phosphonate groups per molecule and ATMP has three, it is the latter which displays a higher inhibition capacity. Such a contrast is also observed in the case of $BaSO_4$ precipitation.[30] Therefore, the effectiveness of a phosphonate to inhibit crystallization would not appear to be based exclusively on electrostatic interactions. For instance, the degree of structural matching between the inhibitor and the mirabilite surface is known to be particularly important (see part e below).

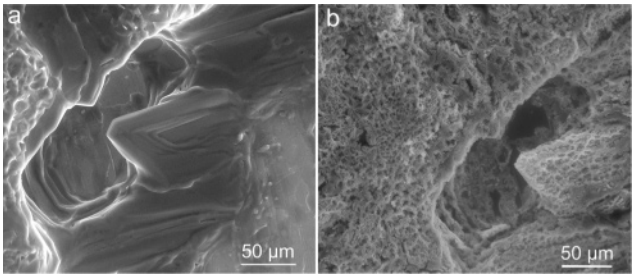

Figure 4. ESEM photomicrographs of sodium sulfate crystals before (a) and after (b) dehydration (i.e., mirabilite → thenardite).

(d) ESEM Study. Mirabilite crystallized in the presence of the three additives and in the control solution. ESEM images showed how newly formed crystals systematically dehydrate after a rise in temperature in the Peltier stage and/or following a reduction in pressure in the ESEM chamber (Figure 4). Such results are consistent with those of XRD, thereby indicating that mirabilite precipitates in all batch crystallization runs.

It is generally accepted that crystallization inhibitors exert their effects through adsorption on active sites (kinks or steps) of a crystal surface.[71] Some inhibitor molecules have the capacity to adsorb on all the crystal faces, decreasing crystallization rates to zero (i.e., nucleation inhibition). They can also preferentially adsorb on specific faces, thus leading to changes in morphology. Such changes are caused by a reduction in the relative growth rates of these faces (i.e., growth inhibition). Those crystal faces on which the additive has been adsorbed later undergo an overdevelopment brought about by the lower growth rates.[72] Our ESEM studies indicate that mirabilite crystals displayed near-equilibrium morphologies in the control (Figure 5a) and in the presence of HEDP (Figure 5b). In contrast, ATMP and DTPMP both induce habit modifications. In particular, the {100} form displays a significant overdevelopment in the presence of the last two additives (Figure 5c−e). This is probably the result of preferential adsorption at these specific faces.

Mirabilite crystals grown in the control solution and in the presence of HEDP were larger than those grown in the presence of ATMP and DTPMP. Crystal density in the presence of ATMP and, in particular, DTPMP was much higher than that of the control or that in the presence of HEDP. These observations point to a higher nucleation density in the presence of ATMP and DTPMP, which substantially increases the number of smaller crystals. This is consistent with crystallization from a highly supersaturated solution.[71] These results suggest that both ATMP and DTPMP act as nucleation and growth inhibitors at moderately alkaline pH (8−8.5).

It is known that additives can influence nucleation processes, generally due to preferential adsorption in growing nuclei whose sizes fall below the critical radius. The crystallization of one of the phases is thus inhibited, while the growth of another is promoted.[73] The presence of heteroatoms in an inhibitor molecule has been reported to increase its inhibition capacity at low pH.[74] At acid pH, the number of deprotonated PO_3^{2-} groups is relatively low (Figure 3). Conversely, nitrogen atoms in DTPMP can be protonated. Such aminophosphonate molecules may therefore easily form hydrogen bonds with the hydration water of mirabilite clusters which cannot exceed the critical size. As a result, mirabilite nucleation is inhibited. On the other hand, the lack of structural water molecules in thenardite favors its crystallization. Interestingly, our ESEM

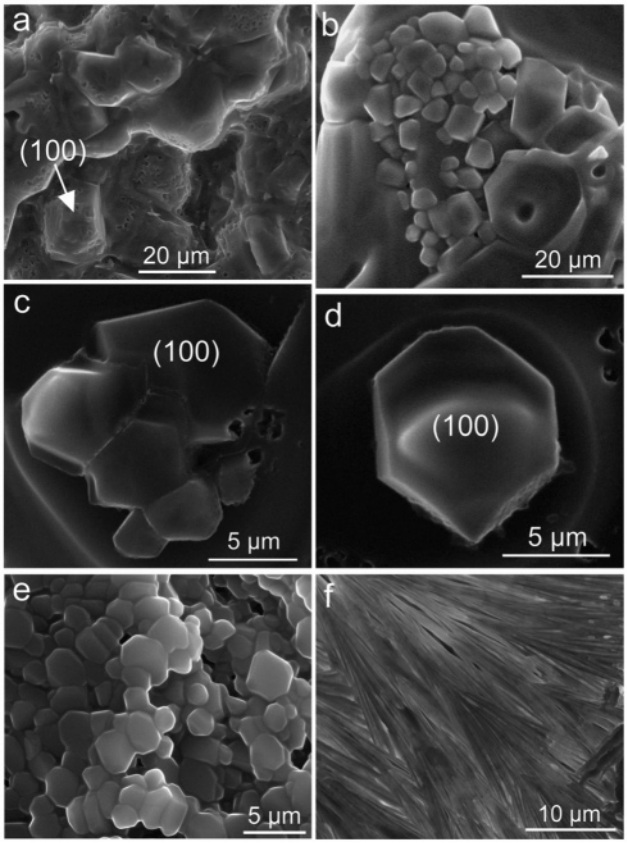

Figure 5. ESEM photomicrographs of sodium sulfate crystals: (a) mirabilite crystals in the control run (the most stable (100) face is indicated); (b) mirabilite formed in the presence of 10^{-3} M HEDP (pH 8); (c) mirabilite crystal with overdeveloped (100) formed in the presence of 10^{-3} M ATMP (pH 8.5); (d) detail of mirabilite {100} form developed in the presence of 10^{-4} M ATMP (pH 8.5); (e) mirabilite crystals with predominant {100} form, developed in the presence of 10^{-3} M DTPMP (pH 8.5); (f) palm-tree/featherlike thenardite crystals formed in the presence of 10^{-3} M DTPMP (pH 3.2).

studies showed that thenardite precipitated directly following the addition of DTPMP (10^{-3} M) with no neutralization of the saline solution (pH 3.4) (Figure 5d). In this case, thenardite crystallization occurs at a high supersaturation, as evidenced by the morphology of the resulting featherlike aggregates (Figure 5f).[75] DTPMP is the only phosphonate that shows this behavior, probably because it has the highest number of heteroatoms.

Apparently, DTPMP acts as an effective crystallization inhibitor at low pH. This latter behavior could thus contribute to the desalination of noncalcareous stones (e.g., sandstones), although it would not be applicable to calcareous stones (the acid pH would lead to carbonate dissolution). In contrast, our results show that ATMP and DTPMP both act as effective crystallization inhibitors at pH 8−8.5 and may therefore be applicable in the desalination of calcareous stones.

(e) Molecular Modeling. Our model for mirabilite borrows the fractional atomic coordinates and site occupancy parameters which appear in the report by Levy and Lisensky.[76] Figure 6 shows the structure of mirabilite as proposed by these authors. The modeling process began by calculating the equilibrium morphology of sodium sulfate decahydrate using the BFDH algorithm. This calculation was performed in order to identify the key growth faces (i.e., those faces which are morphologically more important because they display slower growth rates). The predicted equilibrium morphology is in agreement with the morphology of the mirabilite crystals observed in the ESEM

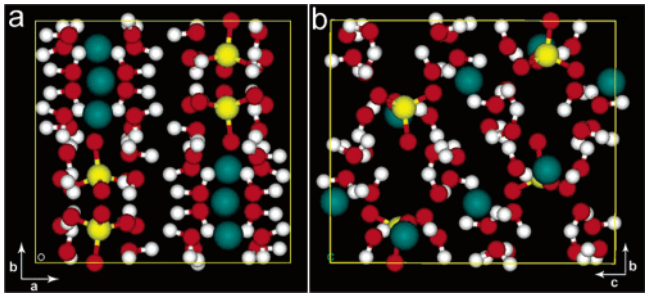

Figure 6. Mirabilite structure: (a) projected on (001); (b) projected on (100). Legend: (blue) Na; (yellow) S; (white) H; (red) O.

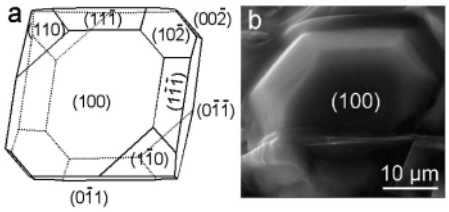

Figure 7. Morphology of mirabilite: (a) calculated (using BFDH method); (b) experimental (ESEM photomicrograph). Note that the {100} faces are those with the highest development.

studies (control runs) (Figure 7). Both the calculated and the observed morphology indicate that the growth of the (100) face is the slowest.

Once the morphology of mirabilite was determined, additive molecules were sketched and afterward optimized using the "Smart Minimizer" with "high convergence" criteria. Their optimal conformation was determined following minimization with respect to energy. The criteria for the high-convergence minimizations are: atom root-mean-square force 0.001 kcal mol^{-1} $Å^{-1}$; atom maximum force 0.005 kcal mol^{-1} $Å^{-1}$; energy difference 1×10^{-4} kcal mol^{-1}; root-mean-square displacement 1×10^{-5} Å; maximum displacement 5×10^{-5} Å. $HEDP^{3-}$, $ATMP^{5-}$, and $DTPMP^{8-}$ were optimized (Figure 8), since these are the main ionic species at pH 8−8.5 (Figure 3).

At least three explanatory hypotheses appear in the literature in order to account for additive−crystal interactions. These hypotheses presuppose that growth inhibition requires at least a bidentate adsorption of the additive on a crystal face. As Black et al.[34] and Bosbach et al.[38] interpreted in the case of barite, first-neighbor sulfate ions may be replaced by the phosphonates tested. According to our results, however, mirabilite surface structure and the distances within the additive molecule make it impossible for there to be a simultaneous substitution of two sulfate ions, especially with regard to the (100) face (Table 3).

Black et al. have also suggested for gypsum crystallization in the presence of impurities that the ionized additives adsorb via H bonding onto the crystal hydration water molecules.[34] When the H−H distances in the mirabilite (100) face and the O−O distances in the additive molecules (Table 4) are compared, all three have at least two possible docking positions on the (100) face. Consequently, all of them could act as growth inhibitors. However, HEDP induces no significant morphology changes in mirabilite crystals and there is no detectable crystallization inhibition at pH 8. H bonding does not, therefore, seem to be the ruling mechanism in mirabilite crystallization inhibition in the presence of phosphonates, although it may contribute to growth inhibition.

Cody and Cody have proposed that the interaction between carboxylic acids and calcium oxalate monohydrate takes place

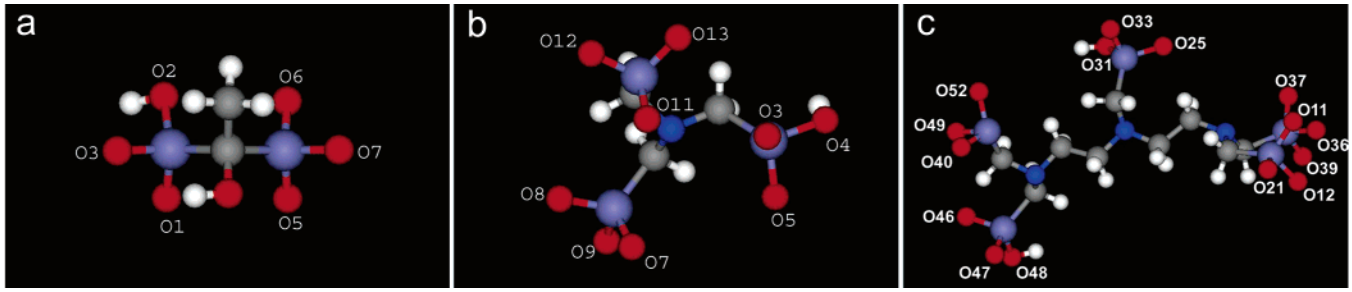

Figure 8. Optimized molecular structures of (a) $HEDP^{3-}$, (b) $ATMP^{5-}$, and (c) $DTPMP^{8-}$. Legend: (light blue) P; (red) O; (dark blue) N; (white) H; (gray) C.

Table 3. Inter-Sulfate and Inter-Phosphorus Distances in Mirabilite and Organophosphonic Acids

mirabilite		phosphonate	
(*hkl*) plane	S−S dist (Å)	additive	P−P dist (Å)
(100)	6.803	ATMP	4.441
	10.380		4.967
	12.830		5.056
(011)	11.510	HEDP	2.989
	16.503		
(110)	7.695	DTPMP	
	7.810		4.115
	12.830		5.051
(11$\bar{1}$)	7.810		6.261
	13.850		7.161
	14.389		7.567
(002)	7.810		8.681
	10.380		11.530
	11.510		11.956
(10$\bar{2}$)	10.380		12.050
	11.565		12.216
	13.945		

Table 4. Comparison of O−O Distances in Optimized Additive Molecules and H−H Distances in Mirabilite (100) Plane

	O−O dist in additive[a] (Å)	H−H dist in mirabilite (100)[b] (Å)	mismatching (%)
$HEDP^{3-}$	5.815 (O7−O3)	5.829 (13b−9b)	0.24
	3.174 (O6−O1)	3.196 (13b−9b)	0.69
$ATMP^{5-}$	7.107 (O12−O5)	7.117 (13b−9b)	0.14
	5.821 (O13−O5)	5.829 (13b−9b)	0.15
$DTPMP^{8-}$	13.858 (O49−O39)	13.838 (13b-9b)	0.14
	13.735 (O40−O37)		0.74
	13.745 (O46−O37)		0.77
	13.794 (O47−O39)		0.31
	12.945 (O47−O36)	12.830 (13b−13b)	0.90
	12.884 (O47−O12)		0.42
	12.619 (O52−O37)	12.576 (13b−9b)	0.34
	9.754 (O33−O36)	9.804 (11a−13b)	0.51
	9.722 (O33−O12)		0.84
	9.206 (O33−O39)	9.133 (11a−9b)	0.70
	9.069 (O33−O21)		0.80
	7.489 (O33−O49)	7.545 (13b−13b)	0.75
	6.789 (O52−O47)	6.808 (9b−9b)	0.30
	6.772 (O36−O21)		0.50
	6.843 (O25−O11)		0.51
	5.815 (O33−O52)	5.829 (13b−9b)	0.25
	3.354 (O39−O11)	3.325 (11a−9b)	0.88
	3.179 (O39−O12)	3.196 (13b−9b)	0.53

[a] Oxygen numbering (in parentheses) corresponds to that shown in Figure 8. [b] Hydrogen nomenclature (in parentheses) corresponds to that shown in Figure 9.

due to the bonding of the additives to cations on crystal surface(s).[77] In the case of $ATMP^{5-}$ and $DTPMP^{8-}$, we found a high structural fit between the additives and the sodium cations present on the mirabilite (100) face (Table 5). However, this fit is not found in $HEDP^{3-}$. Examples of potential docked positions of $ATMP^{5-}$ and $DTPMP^{8-}$ on the (100) cleavage face can be seen in Figures 10 and 11, respectively. This coincides with the results of batch tests performed at moderately alkaline pH, thus showing that ATMP and DTPMP inhibit sodium sulfate decahydrate crystallization, whereas HEDP does not. On the other hand, the molecular modeling is consistent with ESEM observations of overdeveloped {100} forms in mirabilite crystals

Table 5. Na−Na Distances in Different Mirabilite (*hkl*) Planes and O−O Distances in PO_3^{2-} Groups of $ATMP^{5-}$ and $DTPMP^{8-}$ [a]

(*hkl*)	mirabilite	ATMP[b]	DTPMP[b]
(100)	7.013	7.058 (O3−O9, 0.64)	
	9.705		9.754 (O33−O36, 0.50)
			9.722 (O33−O12, 0.17)
	9.749		9.754 (O33−O36, 0.05)
			9.722 (O33−O12, 0.28)
	10.380		10.335 (O33−O47, 0.43)
(110)	7.606		7.640 (O33−O40, 0.44)
		7.902 (O13−O9, 0.04)	7.621 (O25−O52, 0.20)
	7.905		7.884 (O25−O21, 0.26)
	12.830		12.945 (O47−O36, 0.90)
			12.884 (O47−O12, 0.42)
	13.188		13.307 (O52−O12, 0.90)
	13.623		13.639 (O46−O36, 0.12)
			13.563 (O52−O39, 0.44)
			13.715 (O47−O11, 0.68)
			13.735 (O40−O37, 0.82)
			13.510 (O40−O21, 0.83)
			13.745 (O46−O37, 0.90)
(11$\bar{1}$)	7.606		7.640 (O33−O40, 0.44)
			7.621 (O25−O52, 0.20)
	7.905	7.902 (O13−O9, 0.04)	7.884 (O25−O21, 0.26)
	13.188		13.307 (O52−O12, 0.90)
	13.623		13.639 (O46−O36, 0.12)
			13.563 (O52−O39, 0.44)
			13.715 (O47−O11, 0.68)
			13.735 (O40−O37, 0.82)
			13.510 (O40−O21, 0.83)
			13.745 (O46−O37, 0.90)
	14.389		14.354 (O49−O39, 0.24)
			14.305 (O40−O39, 0.58)
(10$\bar{2}$)	10.360		10.335 (O33−O47, 0.24)
	10.380		10.335 (O33−O47, 0.43)
	13.623		13.639 (O46−O36, 0.12)
			13.563 (O52−O39, 0.44)
			13.715 (O47−O11, 0.68)
			13.735 (O40−O37, 0.82)
(002)	7.606		7.640 (O33−O40, 0.44)
			7.621 (O25−O52, 0.20)
	7.905	7.902 (O13−O9, 0.04)	7.884 (O25−O21, 0.26)
	10.380		10.335 (O33−O47, 0.43)

[a] Only O−O distances with less than 1% mismatching have been indicated; no O−O distance in HEDP fulfils this requirement. All distances are given in Å. [b] O−O distance and percent mismatching are given in parentheses. The oxygen numbering corresponds to that shown in Figure 8.

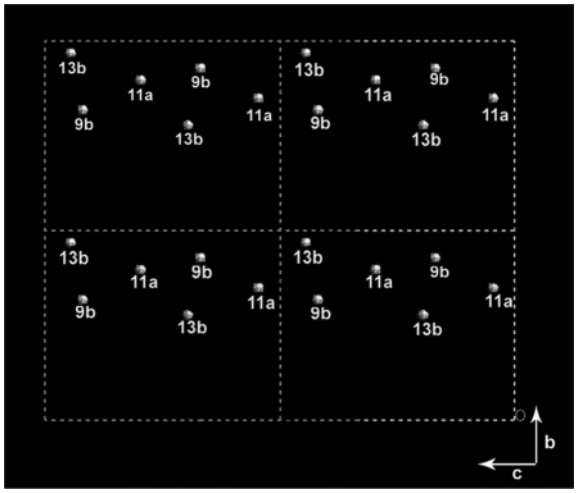

Figure 9. Distribution of H atoms (hydration water) on the mirabilite (100) face (four unit cells are represented).

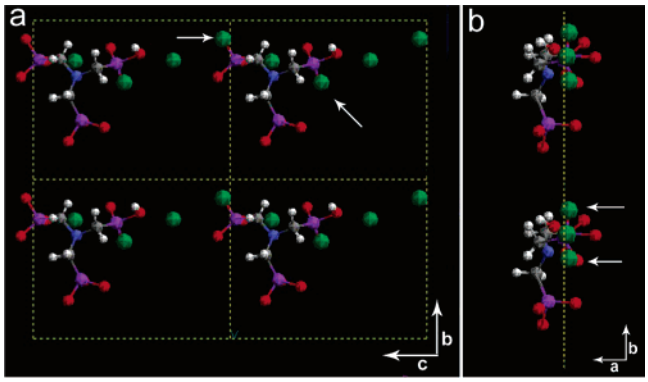

Figure 10. Example of possible docked positions of $ATMP^{5-}$ molecules on mirabilite (100) (four unit cells are shown), giving (a) top and (b) lateral views of the mirabilite (100) surface. For the sake of clarity, only the Na cations of mirabilite have been represented. Arrows indicate bonding between Na and deprotonated functional groups of the phosphonate molecules. Legend: (purple) P; (red) O; (dark blue) N; (white) H; (gray) C; (green) Na.

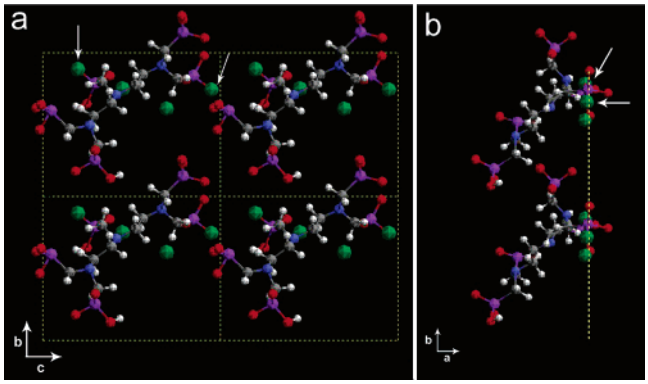

Figure 11. Examples of possible docked positions of $DTPMP^{8-}$ molecules on mirabilite (100) (four unit cells are represented), giving (a) top and (b) lateral views of the mirabilite (100) surface. For the sake of clarity, only Na cations of mirabilite have been represented. Arrows indicate bonding between Na and deprotonated functional groups of the phosphonate molecules. The atom color code is given in Figure 10.

grown in the presence of ATMP and DTPMP. Consequently, we suggest that ATMP and DTPMP inhibit crystallization and growth by blocking the displacement of growth steps. This occurs as a result of adsorption on the mirabilite (100) face via binding to surface sodium ions. Such interaction may be enhanced if hydrogen bonding also participates in the surface binding, as proposed by Zieba et al.[43] for the case of hydroxyapatite.

Conclusions

Promotion of mirabilite crystallization by HEDP, ATMP, and DTMP is significant at pH similar to that of the control solution, particularly in the presence of silicone grease. This is probably due to adsorption and self-assembling of the phosphonates on the substrate, forming a template with the additive functional groups directed toward the bulk solution. Such an effect promotes template-directed heterogeneous nucleation of mirabilite crystals. At neutral pH, the additives tested could therefore minimize damage due to sodium sulfate crystallization in ornamental stones, since they reduce the critical supersaturation and, thus, the crystallization pressure associated with mirabilite crystallization.

The molecular characteristics of DTPMP and ATPM (i.e., molecular conformation and dimensions, as well as chemical composition, which includes phosphonate and amine groups), make them powerful sodium sulfate precipitation inhibitors. This effect is strongly pH dependent (i.e., degree of deprotonation of the functional groups) and, to a lesser extent, concentration dependent. Rises in pH resulted in greater inhibition capacity of additives on sodium sulfate precipitation up to pH ~8.5. Further increases in pH reduced the degree of inhibition. Our results reveal a good structural matching between the additives ATMP and DTPMP and mirabilite {100}, thus leading to additive adsorption onto these faces. As a consequence, ATMP and DTPMP adsorption at moderately alkaline pH produces mirabilite growth inhibition and changes its growth morphology.

At acid pH, DTPMP acts as a powerful nucleation inhibitor, in this case with respect to mirabilite, due probably to H bonding between protonated nitrogen atoms and water molecules of mirabilite clusters whose dimensions are below the critical size. This leads to thenardite precipitation, which only precipitates directly under equilibrium conditions at temperatures of above 32.4 °C.[12a]

These results show that phosphonates may help reduce sodium sulfate damage affecting porous ornamental materials, such as stone used in historic architecture and statuary. From a practical, conservation-oriented point of view, tests should be performed to determine whether a methodology of this type can be implemented to treat salt-affected stones by impregnation with phosphonate solutions at adequate pH. The impregnation methods to be tested are either spraying or poulticing. We propose that phosphonates could soon represent a viable tool for the minimization of salt damage and the promotion of stone desalination.

Acknowledgment. This research was financed by the European Commission VIth Framework Program (Contract No. SSP1-CT-2003-501571) and by research group RNM-179 (Junta de Andalucía, Spain). We thank the CEAMA (Junta de Andalucía-Universidad de Granada) for their assistance with ESEM analysis. The original English manuscript was edited by Marco Bettini.

References

(1) Evans, I. S. *Rev. Geomorphol. Dyn.* **1970**, *19*, 153−177.
(2) Winkler, E. M.; Singer, P. C. *Geol. Soc. Am. Bull.* **1972**, *83*(11), 3509−3513.

(3) Winkler, E. M. *Stone in Architecture: Properties and Durability*. Springer: Berlin, 1994.
(4) Goudie, A. S., Viles, H. A.; Parker, A. G. *J. Arid Environ.* **1997**, *37*, 581−598.
(5) (a) Rodriguez-Navarro, C.; Doehne, E. *Earth Surf. Processes Landforms* **1999**, *24*, 191−209. (b) Rodríguez-Navarro, C.; Doehne, E. *Am. Lab.* **1999**, *31*, 28−35.
(6) Scherer, G. W. *Cem. Concr. Res.* **2004**, *34*, 1613−1624.
(7) Rijniers, L. A.; Pel, L.; Huinink, H. P.; Kopinga, K. *Magn. Reson. Imaging* **2005**, *23*, 273−276.
(8) Scherer, G. W. *Cem. Concr. Res.* **2000**, *30*, 673−675.
(9) Price, C. A. *Stone Conservation: An Overview of Current Research*; The Getty Conservation Institute: Los Angeles, 1996.
(10) Price, C. A.; Brimblecombe, P. In *Preventive Conservation: Practice, Theory and Research*; International Institute for Conservation: London, 1994, pp 90−93.
(11) Lazzarini, L.; Tabasso, M. *Il Restauro della Pietra*; CEDAM: Padova, Italy, 1986.
(12) (a) Rodriguez-Navarro, C.; Doehne, E.; Sebastian, E. *Cem. Concr. Res.* **2000**, *30*, 1525−1534. (b) Rodriguez-Navarro, C.; Doehne, E.; Sebastian, E. *Langmuir* **2000**, *16*, 947−954.
(13) Selwitz, C.; Doehne, E. *J. Cultural Heritage* **2002**, *3*, 205−216.
(14) Rodriguez-Navarro, C.; Fernández, L. L.; Doehne, E.; Sebastian, E. *J. Cryst. Growth* **2002**, *243*, 503−516.
(15) Tantayakom, V.; Fogler, H. S.; Charoensirithavorn, P.; Chavadej, S. *Cryst. Growth Des.* **2005**, *5*, 329−335.
(16) House, W. A. *J. Colloid Interface Sci.* **1987**, *119*, 505−511.
(17) Amjad, Z. *Langmuir* **1991**, *7*, 600−603.
(18) Butt, F. H.; Rahman, F.; Baduruthamal, U. *Desalination* **1995**, *103*, 189−198.
(19) Tadros, T. F.; Mayes, I. *J. Colloid Interface Sci.* **1979**, *72*, 245−254.
(20) Amjad, Z. *Langmuir* **1993**, *9*, 597−600.
(21) Bosbach, D.; Hochella, M. F., Jr. *Chem. Geol.* **1996**, *132*, 227−236.
(22) Badens, E.; Veesler, S.; Boistelle, R. *J. Cryst. Growth* **1999**, *198/199*, 704−709.
(23) Oza, D. H.; Sapre, R. K. *Indian J. Technol.* **1976**, *14*, 435−437.
(24) Öner, M.; Do''an, Ö.; Öner, G. *J. Cryst. Growth* **1998**, *186*, 427−437.
(25) Ralston, P. H. *Mater. Protection Performance* **1972**, *11*, 39−44.
(26) van Rosmalen, G. M. *Chem. Eng. Commun.* **1983**, *20*, 209−233.
(27) Jonasson, R. G.; Rispler, K.; Wiwchar, B.; Gunter, W. D. *Chem. Geol.* **1996**, *132*, 215−225.
(28) Klepetsanis, P. G.; Koutsoukos, P. G. *J. Cryst. Growth* **1998**, *193*, 156−153.
(29) He, S.; Kan, A. T.; Tomson, M. B. *Appl. Geochem.* **1999**, *14*, 17−25.
(30) Jones, F., Oliveira, A. Rohl, A. L. Parkinson, G. M.; Ogden, M. I.; Reyhani, M. M. *J. Cryst. Growth* **2002**, *237−239*, 424−429.
(31) Nowack, B. *Water Res.* **2003**, *37*, 2533−2546.
(32) Guo, J.; Severtson, S. J. *Ind. Eng. Chem. Res.* **2004**, *43*(17), 5411−5417.
(33) Kan, A. T.; Fu, G.; Tomson, M. B. *J. Colloid Interface Sci.* **2005**, *281*(2), 275−284.
(34) Black, S. N.; Bromley, L. A.; Cottier, D.; Davey, R. J.; Dobbs, B.; Rout, J. E. *J. Chem. Soc., Faraday Trans.* **1991**, *87*, 3409−3414.
(35) Xila, A. G.; Mikroyannidis, J.; Koutsoukos, P. G. *J. Colloid Interface Sci.* **1992**, *153*, 538−551.
(36) Butt, F. H.; Rahman, F.; Baduruthamal, U. *Desalination* **1997**, *109*, 323−332.
(37) Bosbach, D.; Hall, C.; Putnis, P. *Chem. Geol.* **1998**, *151*, 143−160.
(38) Bosbach, D.; Coveney, P. V.; Griffin, J. L. W.; Putnis, A.; Risthaus, P.; Stackhouse, S.; Whiting, A. *J. Chem. Soc., Perkin Trans. 2* **2002**, 1238−1245.
(39) Pina, C. M.; Putnis, C. V.; Becker, U.; Biswas, S.; Carroll, E. C.; Bosbach, D.; Putnis, A. *Surf. Sci.* **2004**, *553*, 61−74.
(40) Harmandas, N. G., Navarro Fernandez, E.; Koutsoukos, P. G. *Langmuir* **1998**, *14*, 1250−1255.
(41) Covency, P. V.; Davey, R. J.; Griffin, J. L.; Whiting, A. *Chem. Commun.* **1998**, 1467−1468.
(42) Bishop, M.; Bott, S. G.; Barron, A. R. *Chem. Mater.* **2003**, *15*, 3074−3088.
(43) Zieba, A.; Sethuraman, G.; Pérez, F.; Nancollas, G. H.; Cameron, D. *Langmuir* **1996**, *12*, 2853−2858.
(44) Dirksen, J. A.; Ring, T. A.; Duvall, K. N.; Jongen, N. *Int. J. Refrig.* **2001**, *24*, 856−859.
(45) Ring, T. A.; Dirksen, J. A.; Duvall, K. N.; Jongrn, N. *J. Colloid Interface Sci.* **2001**, *239*, 399−408.
(46) Flatt, R. J. *J. Cryst. Growth* **2002**, *242*, 435−454.
(47) ASTM C 88-90, Standard test method for soundness of aggregate by use of sodium sulfate or magnesium sulfate. In *Annual Book of ASTM Standards*; ASTM: Philadelphia, PA, 1997; Vol. 4, Chapter 2, pp 37−42.
(48) Raleigh, C. W. *Ceram. Bull.* **1991**, *70*, 884−886.
(49) Marliacy, P.; Solimando, R.; Bouroukba, M.; Schuffenecker, L. *Thermochim. Acta* **2000**, *344*, 85−94.
(50) Rappé, A. K.; Casewit, C. J.; Colwell, K. S.; Goddard, W. A.; Skiff, W. M. *J. Am. Chem. Soc.* **1992**, *114*, 10024−10035.
(51) Rappé, A. K.; Colwell, K. S.; Casewit, C. J. *Inorg. Chem.* **1993**, *32*, 3438-.
(52) (a) Casewit, C. J.; Colwell, K. S.; Rappé, A. K. *J. Am. Chem. Soc.* **1992**, *114*, 10035−10046. (b) Casewit, C. J.; Colwell, K. S.; Rappé, A. K. *J. Am. Chem. Soc.* **1992**, *114*, 10046−10053.
(53) Rappé, A. K.; Goddard, W. A. *J. Phys. Chem.* **1991**, *95*, 3358.
(54) Donnay, J. D. H.; Harker, D. *Am. Mineral.* **1937**, *22*, 446.
(55) Agarwal, P.; Berglund, K. A. *Cryst. Growth Des.* **2004**, *4*, 479−483.
(56) Martin, J.; Alcantara, R.; Garcia-Ruiz, J. M. *Cryst. Res. Technol.* **1991**, *26*, 35−42.
(57) Stumm, W.; Morgan, J. J. *Aquatic Chemistry: Chemical Equilibria and Rates in Natural Waters*, 3rd ed.; Wiley: New York, 1996; Chapter 9.
(58) Schukarev, A.; Rosenqvist, J.; Sjöberg, S. *J. Electron Spectrosc. Relat. Phenom.* **2004**, *137−140*, 171−176.
(59) Sverjensky, D. A. *Geochim. Cosmochim. Acta* **2005**, *69*, 225−257.
(60) Kanan, S. M.; Tripp, C. P. *Langmuir* **2002**, *18*, 722−728.
(61) Nowack, B.; Stone, A. T. *J. Colloid Interface Sci.* **1999**, *214*, 20−30.
(62) Pawsey, S.; Yach, K.; Reven, L. *Langmuir* **2002**, *18*, 5205−5212.
(63) D′Andrea, S. C.; Iyer, K. S.; Luzinov, I.; Fedeev, A. Y. *Colloids Surf. B* **2003**, *32*, 235−243.
(64) Addadi, B. L.; Weiner, S. *Angew. Chem., Int. Ed.* **1992**, *31*, 153−169.
(65) Haiduc, I. *Organometallics* **2004**, *23*, 3−8.
(66) Füredi-Milhofer, H.: Sarig, S. *Prog. Cryst. Growth Charact. Mater.* **1996**, *32*, 45−74.
(67) van der Leeden, M. C.; van Rosmalen, G. M. *J. Colloid Interface Sci.* **1995**, *171*, 142−149.
(68) Deluchat, V.; Bollinger, J. C.; Serpaud, B.; Caullet, C. *Talanta* **1997**, *44*, 897−907.
(69) Tomson, M. B.; Kan, A. T.; Oddo, J. E. *Langmuir* **1994**, *10*, 1442−1449.
(70) van der Leeden, M. C.; van Rosmalen, G. M. *Desalination* **1987**, *66*, 185.
(71) Mullin, J. W. *Crystallization*; Butterworth-Heinemann: Oxford, U.K., 1993.
(72) Nancollas, G. H.; Zawacki, S. J. In *Process Technology Proceedings*; Elsevier: Amsterdam, 1984; Vol. 2 (issue: Ind. Cryst.), pp 51−59.
(73) Füredi-Milhofer, H.; Babicivancic, V.; Brecevic, L.; Filipovicvincekovic, N.; Kralj, D.: Komunjer, L.; Markovic, M.; Skrtic, D. *Colloids Surf.* **1990**, *48*, 219−230.
(74) Breen, P. J.; Downs, H. H.; Diel, B. N. *Spec. Publ. R. Soc. Chem.* **1991**, *97*, 186−198.
(75) Sunagawa, I. *Bull. Mineral.* **1981**, *104*, 81−87.
(76) Levy, H. A.; Lisensky, G. C. *Acta Crystallogr., Sect. B: Struct. Sci.* **1978**, *34*, 3502−3510.
(77) Cody, A. M.; Cody, R. D. *J. Cryst. Growth* **1994**, *135*, 235−245.

CG050503M